depends itself on the salt concentration of the solution. In the case of the low molar mass DNA fragments and the salt concentration used in the present investigation, only two of these equations are needed. There are, for $d\phi/dR$

$$d\phi/dR = -(2/R)\{1 - \tfrac{1}{2}\alpha \cot [\tfrac{1}{2}\alpha \ln (R^*/R) + \sin^{-1} (\alpha/e^{1/2}R^*)]\}$$
$$2 \times 10^{-3} \le C_s \le 2 \times 10^{-2} \text{ mol dm}^{-3} \quad \text{(A.5a)}$$

$$d\phi/dR = -(2/R)\{1 + \tfrac{1}{2}\alpha \cot [\tfrac{1}{2}\alpha \ln (R/R^*) + \sin^{-1} (\alpha/e^{1/2}R^*)]\}$$
$$4 \times 10^{-2} \le C_s \le 5 \times 10^{-1} \text{ mol dm}^{-3} \quad \text{(A.5b)}$$

In these equations e is the base of natural logarithms (e = 2.718 28). Note that for (A.5a) R^* must satisfy the condition $0.601\,973 < R^* < 1.552\,651$ and for (A.5b) $R^* > 1.552\,651$. The value of the parameter α can be related to that of R^* through the second condition (A.4).

$$\alpha = \pm\{eR^{*2} - (2 - \{R^*K_1(R^*)/K_0(R^*)\})\}^{1/2} \quad \text{(A.6)}$$

Equations for the derivatives of ϕ have been used here because the value for $d\phi/dR$ at the surface of the polyelectrolyte may be calculated from the surface charge density by using Gauss's law. At the surface where $R = R_0 = \kappa a$

$$(d\phi/dR)_{R=R_0} = -Q\nu/\kappa a \quad \text{(A.7)}$$

Values of R^* may be calculated in an iterative way by using either (A.5a) or (A.5b). Once R^* is known, ν_{eff} may be calculated from eq 17 with $B^{-1} = K_0(R^*)$.

References and Notes

(1) Brenner, S. L.; Parsegian, A. V. *Biophys. J.* **1976**, *17*, 327.
(2) Stigter, D. *Biopolymers* **1977**, *16*, 1435.
(3) Fixman, M.; Skolnick, J. *Macromolecules* **1978**, *11*, 863.
(4) Stroobants, A.; Lekkerkerker, H. N. W.; Odijk, T. *Macromolecules* **1986**, *19*, 2232.
(5) Onsager, L. *Ann. N.Y. Acad. Sci.* **1949**, *51*, 627.
(6) Elias, J. G.; Eden, D. *Macromolecules* **1981**, *14*, 410.
(7) Yamakawa, A. *Modern Theory of Polymer Solutions*; Harper & Row: New York, 1971.
(8) Tsihara, A. *J. Chem. Phys.* **1950**, *18*, 1446.
(9) Isihara, A.; Hayashida, T. *J. Phys. Soc. Jpn.* **1951**, *6*, 40.
(10) Manning, G. S. *J. Chem. Phys.* **1969**, *51*, 924.
(11) Anderson, C. F.; Record, M. T. *Annu. Rev. Phys. Chem.* **1970**, *33*, 191.
(12) Ramanathan, G. V.; Woodbury, C. P. *J. Chem. Phys.* **1982**, *77*, 4133.
(13) Philip, J. R.; Wooding, R. A. *J. Chem. Phys.* **1970**, *52*, 953.
(14) Fixman, M. *J. Chem. Phys.* **1979**, *70*, 4995.
(15) Skolnick, J.; Grimmelman, E. K. *Macromolecules* **1980**, *13*, 335.
(16) Katoh, T.; Ohtsuki, T. *J. Polym. Sci., Polym. Phys. Ed.* **1982**, *20*, 2167.
(17) Shindo, H.; Mc Ghee, J. P.; Cohen, J. S. *Biopolymers* **1980**, *19*, 523.
(18) Nicolai, T.; van Dijk, L.; van Dijk, J. A. P. P.; Smit, J. A. M. *J. Chromatogr.* **1987**, *389*, 286.
(19) Hirshman, S. Z.; Felsenfeld, G. *J. Mol. Biol.* **1986**, *16*, 347.
(20) Mandel, M.; Varkevisser, F. A.; Bloys van Treslong, C. J. *Macromolecules* **1982**, *15*, 675.
(21) Mandel, M.; Schouten, J. *Macromolecules* **1980**, *13*, 1247.
(22) Mandelkern, M.; Dattagupta, N.; Crothers, D. M. *Proc. Natl. Acad. Sci. U.S.A.* **1981**, *87*, 4294.
(23) Vreugdenhil, Th.; van der Touw, F.; Mandel, M. *Biophys. Chem.* **1979**, *10*, 67.
(24) Fulmer, A. W.; Benbasat, J. A.; Bloomfield, V. A. *Biopolymers* **1981**, *20*, 1147.
(25) Härd, T.; Kearns, D. R. *Biopolymers* **1986**, *25*, 1519.
(26) Elias, J. G.; Eden, D. *Biopolymers* **1981**, *20*, 2369.
(27) Schellman, J. A.; Stigter, D. *Biopolymers* **1977**, *16*, 1415.
(28) Odijk, T. *J. Polym. Sci., Polym. Phys. Ed.* **1977**, *15*, 477.
(29) Skolnick, J.; Fixman, M. *Macromolecules* **1977**, *10*, 944.
(30) Odijk, T.; Houwaart, A. C. *J. Polym. Sci., Polym. Phys. Ed.* **1978**, *16*, 627.

Kinetics of Isothermal Crystallization and Curie Transition of the 81/19 mol % Vinylidene Fluoride–Tetrafluoroethylene Copolymer

Hervé Marand* and Richard S. Stein

Polymer Research Institute, University of Massachusetts, Amherst, Massachusetts 01003.
Received February 27, 1988; Revised Manuscript Received June 28, 1988

ABSTRACT: The kinetics of crystallization and Curie transition of the 81/19 mol % vinylidene fluoride–tetrafluoroethylene (VF_2–F_4E) copolymer are investigated for different isothermal conditions by wide-angle X-ray diffraction, small-angle light scattering, and differential scanning calorimetry. The results of this study indicate that, in agreement with previous investigations, the isothermal crystallization from the melt produces first the paraelectric crystal phase. The paraelectric phase is observed to undergo isothermally a crystal–crystal transition into the ferroelectric phase. Examination of the melting behavior of samples crystallized for different lengths of time indicates that the ferroelectric phase does not undergo any crystal–crystal transition upon heating, as was suggested by other investigators, but melts at a temperature about 10 deg higher than the original paraelectric phase. The crystallization and crystal–crystal transition kinetics are extremely temperature dependent and the ratio of the crystallization rate to Curie transition rate increases with crystallization temperature.

Introduction

Considerable work has been carried out in the past few years to investigate the existence and characteristics of the Curie transition in poly(vinylidene fluoride) (PVF_2) and related copolymers.[1-28] The intrinsic ferroelectric nature of PVF_2 was first suggested by the observation of a ferro- to paraelectric transition in vinylidene–trifluoroethylene copolymers (VF_2–F_3E) of various VF_2 mole fractions.[1-17] Lovinger et al.[7,8] proposed a value of 205 °C for the Curie temperature of PVF_2 by extrapolation of X-ray and dielectric data for VF_2–F_3E copolymers to 100% VF_2 content. To avoid any ambiguity in the interpretation of the data as a result of the alteration of the chemical structure of PVF_2 by a different chemical species (F_3E) (difference in

* To whom correspondence should be addressed at Virginia Polytechnic Institute and State University, Chemistry Department, Blacksburg, VA 24061.

0024-9297/89/2222-0444$01.50/0

tacticity or regicity), copolymers of vinylidene fluoride and tetrafluoroethylene (VF_2–F_4E) were examined.[18-27] In the latter case, the presence of F_4E units is analogous to an increase in the number of head-to-head (HH) linkages in PVF_2 homopolymer. However, it should be noted that in PVF_2, conversely to the VF_2–F_4E copolymer, each HH linkage is followed by a tail-to-tail (TT) linkage, these HH–TT defects amounting to 3.5–6% in commercial PVF_2. Studies similar to these carried out on the VF_2–F_3E copolymer yielded an extrapolated Curie temperature of 196 °C for pure PVF_2 and demonstrated that the Curie temperature of the copolymer increases linearly with VF_2 content up to around 81/19 mol % fraction, where the Curie transition is aborted by melting.[21,24-26]

More recently, Lovinger et al.[28] were able to synthesize PVF_2 homopolymers of various HH–TT content between 0.2 and 23.5 mol % and to demonstrate unequivocally the existence of the Curie transition in pure PVF_2, when the HH–TT content is between 13.5 and 15.5%. For commercially available PVF_2 grades, the lower amount of HH–TT defects raises the Curie transition above the melting temperature, preventing the observation of the ferro- to paraelectric transition.

In any case, the F_3E or F_4E units and the HH–TT linkages act as defects copolymerized with VF_2 monomers. As a result of the chemical defects in the chain, the crystal packing efficiency decreases, reducing the steric and electrostatic repulsions between neighboring segments. Such a decrease in interchain interaction favors at low temperature the all trans conformation (ferroelectric phase) as opposed to the usually obtained TGTG′ conformation of the α crystal phase. A concomitant effect of the chemical defects is the reduction of the Curie temperature below the melting transition of the ferroelectric phase for large defect contents.[7,8,24-26,28]

Most of the investigations of the crystallization from the melt and the incipient Curie transition in VF_2–F_4E systems have been focussed on the 81/19 mol % composition.[18-27] Results from differential scanning calorimetry (DSC), wide-angle X-ray diffraction (WAXD) and dielectric studies have suggested that by cooling from the melt this particular copolymer crystallizes into the paraelectric phase and then undergoes a crystal–crystal transition into the ferroelectric phase upon further cooling. The Curie transition was reported to exhibit a hysteresis and to be observed at higher temperature during heating runs than during cooling runs.[21-27] For the 81/19 mol % copolymer composition, however, the Curie transition lies in the vicinity of the melting transition and competition between crystallization and crystal–crystal transition should be expected to affect the content in various crystalline phases. In this study, wide-angle X-ray diffraction, small-angle light scattering (SALS) and differential scanning calorimetry will be used to estimate the kinetics of crystallization and Curie transition (para- to ferroelectric crystal transition) in isothermal conditions.

Experimental Section

Samples of 81/19 mol % (73/27 wt %) VF_2–F_4E random copolymers (Kynar 7200) were kindly supplied by Pennwalt Corp.

For the WAXD studies, the copolymer sample was placed in a thin wall capillary tube 2 mm in diameter and mounted in a hot stage with thin mica windows. The diffraction studies were carried out on a four-circle Siemens diffractometer, Model D-500, operated in the transmission mode with Nickel-filtered Cu Kα radiation (λ = 1.542 Å). $\theta/2\theta$ scans between 17° and 21° 2θ angles were recorded at different times during the isothermal crystallization.

For the SALS studies, 20-μm thick compression molded films were prepared. The films were inserted between glass slide and cover slip, mounted in a Mettler hot stage type FP 2, melted at 200 °C for 10 min, and quenched to the desired crystallization temperature. The samples were allowed to crystallize isothermally for different lengths of time and were then heated from the crystallization temperature up to 200 °C at a 2 °C/min rate. During both the isothermal crystallization and the melting, SALS patterns were obtained in H_v[29] conditions with a monochromatic He/Ne laser light (λ = 632.8 nm). The patterns were recorded digitally by means of a two-dimensional position sensitive detector interfaced with an optical multichannel analyzer (OMA3).[30,31]

For the DSC experiments, as received samples of weight 10 mg were used. The thermal behavior was studied in a Perkin-Elmer differential scanning calorimeter, Model DSC-2, operating under N_2 atmosphere. The differential heat flux was recorded as a function of time during both crystallization and melting. The crystallization experiments were carried out at 117, 118.5, and 122 °C for different lengths of time and the melting behavior was followed by heating the sample at a 10 °C/min rate (unless otherwise specified) from the crystallization temperature. To ensure that the experimental results were not affected by thermal degradation, new copolymer samples were used at the beginning of every DSC run. Indium and tin standards were used to calibrate the temperature scale and heats of fusion. Overlapping endotherms were deconvoluted in the same manner for all DSC traces by considering the shape of the endotherms at early and late stage of crystallization (when only one of the endotherms is present) and by ensuring that the sum of the differential heats of the deconvoluted endotherms yields the differential heat of the original endotherm at all points. Where the overlap was important, different shapes for the low-temperature tail of the endotherms were considered (cf. error bars on Figure 7a–c). This enabled us to ensure that the deconvolution process was not too sensitive to the author's subjectivity. For the study of the effect of heating rate on the melting behavior (Figure 8), the ordinate axis (dQ/dt) of each DSC trace has been scaled differently for convenience in the data display. What matters in these curves is not the absolute total enthalpy, which did not vary with heating rate, but the ratio of the first to second endotherm for each trace.

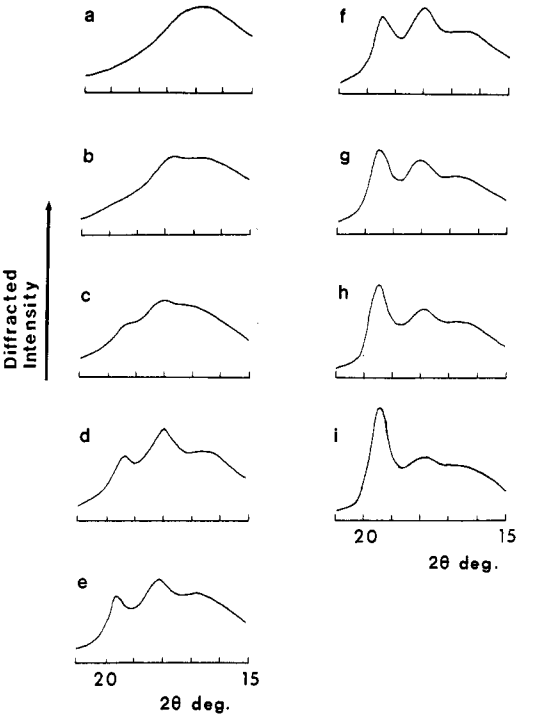

Figure 1. Wide-angle X-ray diffractograms as a function of crystallization time at 124 °C; (a) 30 min, (b) 3 h, (c) 6 h, (d) 20 h, (e) 36 h, (f) 45 h, (g) 60 h, (h) 90 h, (i) 120 h.

Results

Wide-Angle X-ray Diffraction. Crystallization of the 81/19 mol % copolymer was carried out at 124 ± 1 °C. $\theta/2\theta$ scans recorded during the isothermal crystallization

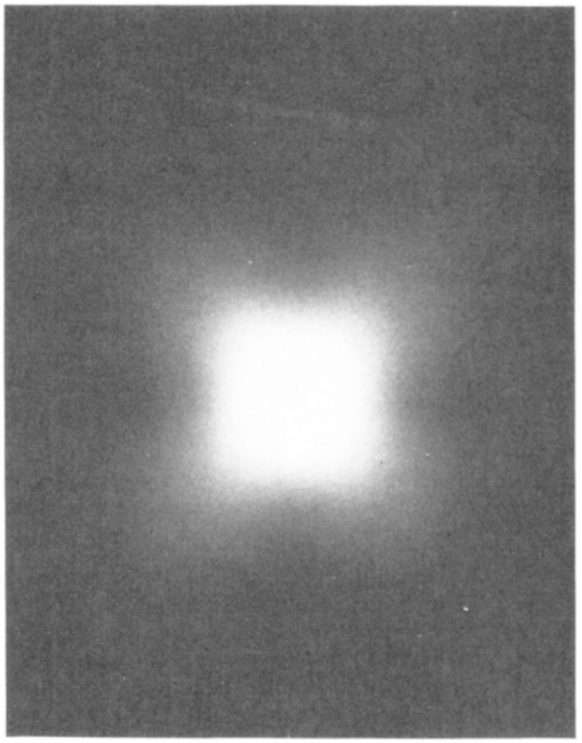

Figure 2. H_v SALS pattern of copolymer sample crystallized at 117 °C. The polarization directions are horizontal and vertical.

are shown on Figure 1. In agreement with Lovinger et al.,[22-25] the first crystalline phase to be produced by crystallization from the melt is the paraelectric phase as evidenced by its reflection around 18° (d = 4.85 Å). The intensity of this reflection is first seen to increase with time and then to decrease after approximately 36 h. The reflection characteristic of the ferroelectric phase (19.6° 2θ) appears only after 6 h of crystallization and steadily increases in intensity with time. The time dependence of the intensities characteristic of the ferro- and paraelectric phase indicates that after being formed, the paraelectric phase transforms into the ferroelectric phase by crystal–crystal transition. Because of the unavailability of the structure factors for either the paraelectric phase or the ferroelectric phase and the lack of knowledge concerning the crystallization and Curie transition rates, it was not possible to derive from the X-ray data the amount of para- and ferroelectric phases at any time and therefore not possible to estimate whether or not part of the ferroelectric phase is formed by direct crystallization from the melt. Because of the very slow transition rate at this temperature, it was not possible to observe the total conversion of the para- to ferroelectric phase in a reasonable experimental time. On the other hand, because of the slow cooling rate achievable in this hot stage and also because of the rather low flux of the X-ray source, it was not possible to study this process at a lower temperature where the crystallization process takes place in a shorter time.

Small-Angle Light Scattering. Examination of the H_v SALS patterns of the samples crystallized at 117 °C indicates that the intensity of maximum scattering is located at zero scattering angle (Figure 2). Although the details of the analysis of the H_v SALS patterns as a function of crystallization temperature and comonomer content will be given in a separate publication,[32] it can already be said that the morphology consists of incomplete spherulites, rodlike crystal agregates and hedrites. Although, for a fully developed spherulitic morphology, it is usually possible to relate quantitatively the maximum

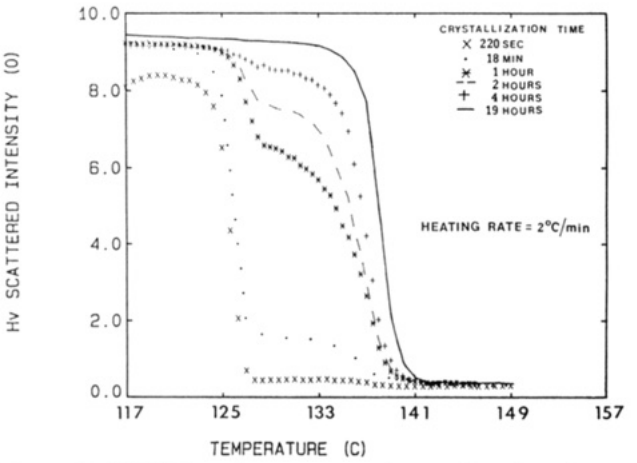

Figure 3. SALS intensity at zero angle as a function of temperature during heating run (2 °C/min) for different crystallization times at 117 °C.

scattering intensity to a "degree of crystallinity",[33] such is not the case, yet, for any different morphology.

It has been shown that, for rodlike crystal agregates, the H_v scattered intensity falls off with scattering angle θ.[34] It was also demonstrated that both the rate of intensity fall with scattering angle and the azimuthal angle (μ) dependence of the scattering are dependent on the orientation correlation function of the crystal optic axes. Considering the particular scattering profile of this material (Figure 2), it was convenient to follow the crystallization and melting processes by monitoring the depolarized transmitted intensity (in the present case, the scattered intensity at zero scattering angle). One has to be aware that during an actual measurement of the intensity of transmitted depolarized light, one actually measures the total integrated scattered intensity in a small solid angle about the undeviated transmitted beam[32] (as a result of the finite aperture of the photomultiplier's tube or the finite surface of the photodiode array used for detection). In the present study, a two-dimensional photodiode array was used to record the time evolution of the scattering pattern and the maximum scattering angle contributing to the measured depolarized light transmission was estimated to be about 0.5°. For such experimental condition, one can assume that the major contribution to the intensity of depolarized transmitted light arises from pure transmission. It was demonstrated by Clough et al.[35] that for a randomly oriented set of crystal agregates, the depolarized transmitted light intensity T can be written as

$$T = (1/2)(N_s A_{cs}/A_0) \sin^2 (\delta/2)$$

where N_s is the number of correlated regions (agregates), A_{cs} is the correlated area for one of the N_s structures, A_0 is the field area containing the N_s structures, δ is the crystal birefringence (for a uniaxial crystal). Although the term $N_s A_{cs}/A_0$ is not rigorously equal to the degree of crystallinity, its variation during crystallization or melting reflects the behavior of the crystallinity.

The copolymer sample was crystallized at 117 °C and heated up to 200 °C after crystallization for different lengths of time. The H_v SALS patterns were recorded during the crystallization and during the heating runs (2 °C/min) at regular time intervals, and the intensity at zero angle was measured as a function of temperature and crystallization time. Figure 3 clearly shows that, for both very short and very long crystallization times, only one single melting process is observed (respectively at 128 and 137 °C). These experiments also indicate that the amplitude of the first melting process (around 128 °C) con-

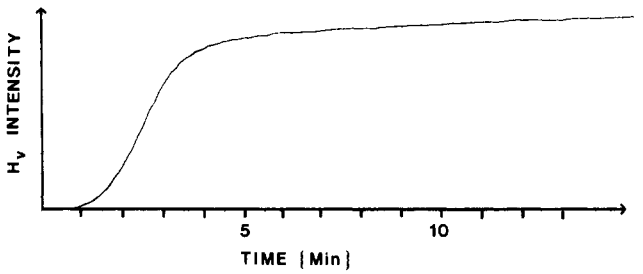

Figure 4. SALS intensity at zero angle as a function of time during crystallization at 117 °C.

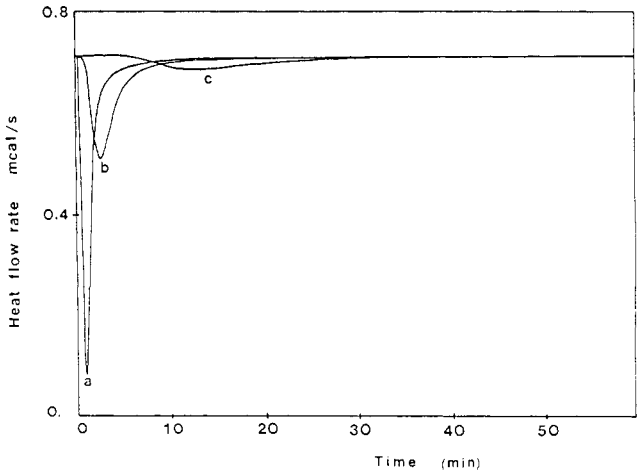

Figure 5. Crystallization exotherms at 117 °C (a), 118.5 °C (b), and 122 °C (c).

tinuously decreases with crystallization time whereas the amplitude of the second melting process continuously increases with crystallization time. These results are consistent with the WAXD data and unambiguously indicate the existence of a crystal–crystal transition subsequent to crystallization of the paraelectric phase. By comparison of the time dependence of the amount in crystal phase (either para- or ferroelectric phase) (crystallization curve, Figure 4) with the time dependence of the Curie transition, one can readily see that the rate of the Curie transition is much slower than the rate of crystallization.

Finally, it must be noted that the first fall in transmitted intensity corresponds to the melting of the paraelectric phase (around 128 °C) and not to the observation of the Curie transition as was reported earlier.[22,23,26] A crystal–crystal transition cannot occur during the heating run since no melting process is observed after the first intensity fall at early crystallization time. Furthermore, a crystal–crystal transition is not expected to produce such a large decrease in scattered intensity. The second fall in transmitted intensity corresponds to the melting of the ferroelectric phase and takes place at a higher temperature (around 137 °C). Further elaboration on these points will be provided after examination of the DSC results.

Differential Scanning Calorimetry. The crystallization behavior was also investigated by differential scanning calorimetry between 117 and 122 °C. Figure 5 shows the crystallization isotherms for 117, 118.5, and 122 °C. The rate of the primary crystallization is seen to be extremely temperature dependent. For temperatures lower than 117 °C, the crystallization could not be prevented during the cooling from the melt whereas above 122 °C the crystallization is so slow that no detectable change in the heat flow rate could be measured. The approximate time for completion of the primary crystallization step is approximatively 7, 21, and 90 min at respectively 117, 118.5, and 122 °C. If we now consider more specifically the

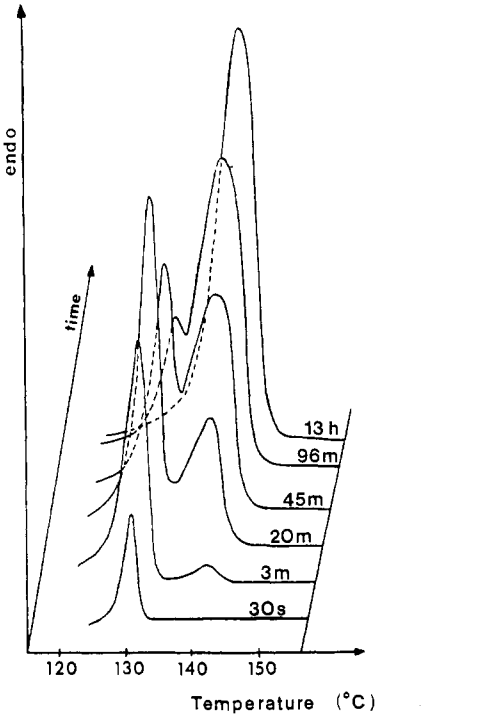

Figure 6. Melting behavior for samples crystallized at 117 °C for different lengths of time.

crystallization behavior at 117 °C and carry out heating runs after various crystallization times, we can see the thermal behavior depicted in Figure 6. The time evolution of the melting behavior for samples crystallized isothermally exhibits three different regimes. For very short crystallization times, one single endotherm is observed around 131 °C. In the first regime, the enthalpy of fusion is observed to increase with crystallization time, indicating the primary crystallization of the paraelectric phase. In the intermediate time range, the enthalpy of melting of the first endotherm is still increasing with time, while a second endotherm appears at higher temperature (ca. 140 °C). This latter endotherm is attributed to the melting of the ferroelectric phase. The end of the second time range (where the enthalpy of fusion of the paraelectric phase is maximum) corresponds closely to tail of the primary crystallization exotherm. In the last stage, the enthalpy of fusion of the paraelectric phase keeps decreasing while that of the ferroelectric phase steadily increases. This indicates that the paraelectric phase has transformed into the ferroelectric phase by isothermal crystal–crystal transition. The same behavior is observed for crystallization at 118.5 and 122 °C. From the heating curves of samples crystallized for different lengths of time, an estimate of the heat of fusion for each melting peak can be obtained as a function of crystallization time (Figure 7a–c). These results indicate that the degree in paraelectric phase crystallinity, achieved during primary crystallization, decreases notably when the crystallization is carried out at higher temperature. The observation of low Curie transition rates for the investigated crystallization temperatures seems quite expected in view of the fact that no exotherm could be observed for the crystal–crystal transition at intermediate and long time of crystallization. Furthermore, the Curie transition enthalpy is certainly much smaller than the enthalpy of fusion. It is unfortunately not possible to deduce from Figure 7a–c the time dependence of the degree of crystallinity in either paraelectric or ferroelectric phase since the enthalpy of fusion for either pure phase is unknown. Such information would allow for the determination of the temperature dependence

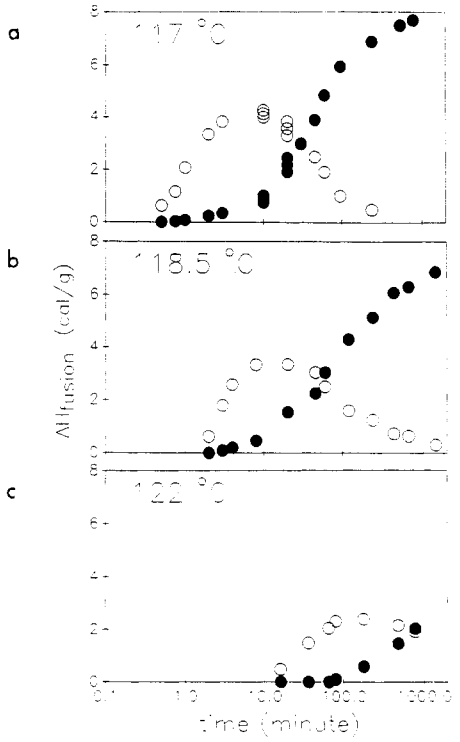

Figure 7. Heat of fusion of paraelectric (○) and ferroelectric (●) phases as a function of crystallization time at (a) 117 °C, (b) 118.5 °C, and (c) 122 °C.

of the Curie transition rate from the data presented above. Extrapolation of the transition rate to zero rate should give an estimate of the "equilibrium Curie temperature" $T_c°$ above which the paraelectric phases crystallizes without undergoing a crystal–crystal transition to the ferroelectric phase. Qualitative examination of Figure 7a–c suggests that the ratio of the rate of crystallization to the rate of Curie transition increases with crystallization temperature.

The effect of heating rate on the melting behavior of the para- and ferroelectric phases was also investigated by DSC for a sample crystallized at 118.5 °C for 18 min. For this time and temperature conditions, no noticeable further crystallization should take place during the heating runs (even at the lowest heating rate investigated). Figure 8 shows the DSC traces for the melting of identical samples at rate between 2.5 and 40 °C/min. The paraelectric phase melting peak is seen to shift markedly to higher temperatures (by 10 °C) when the heating rate is increased from 2.5 to 40 °C/min. On the other hand, the ferroelectric phase melting peak is only shifted by 4 deg in the same range of heating rates. The heat of fusion of either endotherm does not vary with heating rate indicating that no change in the phase content (by melting recrystallization or crystal–crystal transition) is taking place during the heating run from the temperature T_c for a sample crystallized at T_c.

Discussion

In agreement with previous investigations,[22-25] our results indicate that the paraelectric crystal phase is produced from the melt by isothermal crystallization of the (81/19) mol % VF_2–F_4E copolymer in the range 117–124 °C. This study has also demonstrated that the paraelectric phase transforms isothermally into the ferroelectric phase at the crystallization temperature and has suggested that the rate of transformation decreases with increasing temperature. Furthermore, our investigation has shown that, up to at least 124 °C, the para- to ferroelectric transition can be observed within a reasonable time span. This implies that the equilibrium Curie temperature must be higher than 124 °C and that the ferro- to paraelectric phase transition should not be observed at temperatures lower than about 125 °C unless the ferro- to paraelectric transition temperature depends markedly on the temperature at which the ferroelectric phase was formed. No such evidence is available in the literature. The existence of such a ferro- to paraelectric transition for the 81/19 mol % composition has been much debated in the past.[18-27] In the study by Hicks et al.[18] and Tasaka et al.[20] no Curie transition was observed. On the other hand, Lovinger et al.[22-25] and Green et al.[27] have reported the observation of the ferro- to paraelectric transition, respectively, at 110–120 °C for the former group by a combination of WAXD, DSC, and dielectric relaxation and around 113–118 °C by Raman scattering and DSC for the latter. These results are a priori inconsistent with our experimental observations (no transformation between ferro and paraelectric phases was observed during heating at rates from 2.5 to 40 °C/min) and are also inconsistent with the fact that the ferroelectric to paraelectric phase transition is expected to take place at much higher temperature.

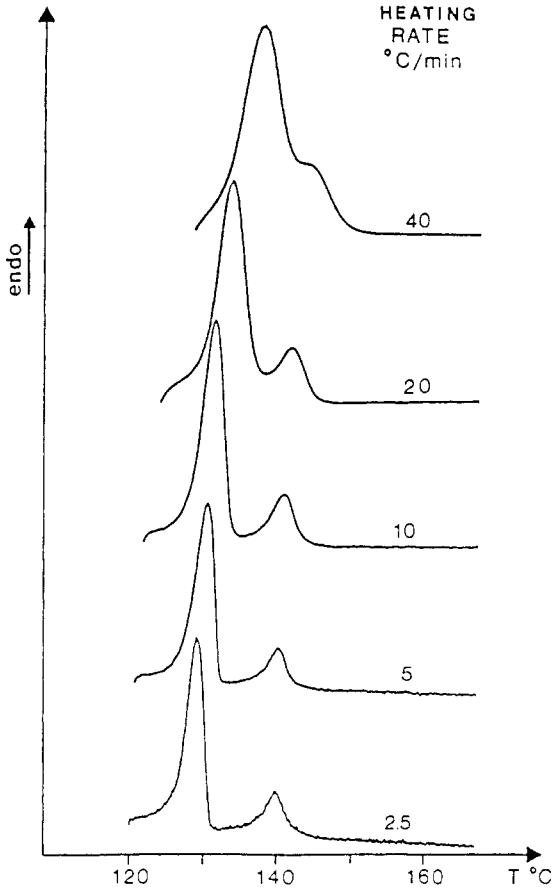

Figure 8. Effect of heating rate of the melting behavior of samples crystallized at 118.5 °C for 18 min.

It is possible to provide an alternate interpretation of their results by examining carefully the experimental procedure used to suggest the existence of the ferro- to paraelectric transition. The samples were either crystallized isothermally and further quenched to room temperature[23] or to lower temperature[27] or were directly cooled from the melt.[21,22,26] In all cases, as was shown here and elsewhere,[22-25] the ferroelectric phase was produced. For a sample crystallized isothermally for one day at T = 117.0 °C and heated from T up to 200 °C, the enthalpy of fusion amounts to about 6–7 cal/g (cf. Figure 7a) which is half of the value obtained for a sample cooled at constant

cooling rate from the melt down to room temperature.[22,23] This suggests that this copolymer will not completely crystallize in isothermal conditions and will further crystallize upon cooling. It is therefore reasonable to suggest that the crystals grown from the melt or from the amorphous phase at the lowest temperature will melt first during the heating run and will have the chance to recrystallize rapidly into the paraelectric phase. When the melting–recrystallization process occurs at low temperature (100–110 °C), the subsequent formation of the ferroelectric phase by crystal–crystal transition is relatively fast. At higher temperature (120 °C and above) the crystal–crystal transition becomes much slower (cf. this work) and the crystallized material remains in the paraelectric phase. Any technique (such as WAXD) that can follow the content in both crystal phases as a function of temperature could in principle prove this hypothesis. We believe that the X-ray data obtained by Lovinger et al.,[23] although it was interpreted differently, is indeed consistent with our explanation. They examined the same copolymer composition crystallized for 1 day at 120 °C and subsequently quenched to room temperature. They obtained diffractograms from such samples heated at 2 °C/min with the temperature of each X-ray scan held isothermal. They reported that heating above 100 °C caused a gradual decrease in the intensity of the ferroelectric phase reflection at 19.6° 2θ, while the reflection characteristic of the paraelectric phase only appeared around 122–129 °C and never reached the same intensity as the ferroelectric phase. Our scenario suggests why there is a delay between the decrease in the intensity of the ferroelectric phase reflection and a very small increase in the intensity of the paraelectric phase reflection. It also gives an alternate explanation for the low intensity of the paraelectric phase reflection observed during heating. A similar line of reasoning can be held against the Raman and DSC data of Green et al.[27] and the DSC and dielectric data of Murata et al.[21,26] Although it was recognized by the previous investigators that the melting of the ferroelectric phase would hinder any clear observation of the ferro- to paraelectric transition, the explanation of the formation of the paraelectric phase in terms of a melting–recrystallization mechanism had been overlooked. We believe that all previous "evidences" of a ferro- to paraelectric transition for the 81/19 mol % composition[21-27] can be reanalyzed according to such a mechanism.

These considerations fully justify the necessity to study these phenomena in isothermal conditions and to examine any multiple transition behavior without any cooling or quenching to room temperature in the case of an easily crystallizable material. This study is not, in any way, inconsistent with the results obtained for VF_2–F_4E copolymers having a larger content in tetrafluoroethylene units, since for these compositions the melting and the Curie transition are well separated and easily characterized.[24,25] However, it showed a more rigorous way to obtain the "equilibrium" Curie temperature as a function of comonomer content, through the temperature dependence of the Curie transition rate. Work is in progress to measure such a temperature dependence for various F_4E contents.

Conclusion

The study of the kinetics of crystallization indicates that in agreement with the work of Lovinger et al.[22,23] the copolymer principally crystallizes from the melt in the paraelectric phase. The Curie transition was found to take place in isothermal condition subsequently to crystallization and at a rate that strongly depends on the temperature. Our results suggest that the ratio of crystallization rate to Curie transition rate increases with temperature. Finally, in contrast with the results of previous investigations,[21-27] our study of the melting behavior indicates that for this copolymer composition, no ferro- to paraelectric crystal transition is observed during heating prior to melting. It is suggested that previous "evidence" of a ferro- to paraelectric transition during heating can be reinterpreted in terms of a melting–recrystallization process.

Acknowledgment. We wish to thank Dr. Philip Bloomfield of Pennwalt Corp. for kindly providing the VF_2–F_4E copolymer samples.

Registry No. $(VF_2)(F_4E)$ (copolymer), 25684-76-8.

References and Notes

(1) Yagi, T.; Tatemoto, M.; Sako, J. *Polym. J.* **1980**, *12*, 209.
(2) Tashiro, K.; Takono, K.; Kobayashi, M.; Chatani, Y.; Tadokoro, H. *Polymer* **1981**, *22*, 1312.
(3) Furukawa, T.; Johnson, G. E.; Bair, H. E.; Tajitsu, Y.; Chiba, A.; Fukada, E. *Ferroelectrics* **1981**, *32*, 61.
(4) Yamada, T.; Ueda, T.; Kitayama, T. *J. Appl. Phys.* **1981**, *52*, 948.
(5) Lovinger, A. J.; Davis, G. T.; Furukawa, T.; Broadhurst, M. G. *Macromolecules* **1982**, *15*, 323.
(6) Davis, G. T.; Furukawa, T.; Lovinger, A. J.; Broadhurst, M. G. *Macromolecules* **1982**, *15*, 329.
(7) Lovinger, A. J.; Furukawa, T.; Davis, G. T.; Broadhurst, M. G. *Ferroelectrics* **1983**, *50*, 227.
(8) Lovinger, A. J.; Furukawa, T.; Davis, G. T.; Broadhurst, M. G. *Polymer* **1983**, *24*, 1225.
(9) Lovinger, A. J.; Furukawa, T.; Davis, G. T.; Broadhurst, M. G. *Polymer* **1983**, *24*, 1233.
(10) Tashiro, K.; Takano, K.; Kobayashi, M.; Chatani, Y.; Tadokoro, H. *Polymer* **1984**, *25*, 195.
(11) Tashiro, K.; Takano, K.; Kobayashi, M.; Chatani, Y. *Ferroelectrics* **1984**, *57*, 297.
(12) Tashiro, K.; Nakamura, M.; Kobayashi, M.; Chatani, Y.; Tadokoro, H.; *Macromolecules* **1984**, *17*, 1452.
(13) Odajima, A.; Tashiro, K. *J. Crystallogr. Jpn.* **1984**, *26*, 103.
(14) Tashiro, K.; Kobayashi, M. *Polymer* **1986**, *27*, 667.
(15) Legrand, J. F.; Schuele, P. J.; Schmidt, V. H.; Minier, M. *Polymer* **1983**, *26*, 1683.
(16) Green, J. S.; Farmer, B. L.; Rabolt, J. F. *J. Appl. Phys.* **1986**, *60*, 2690.
(17) Green, J. S.; Rabe, J. P.; Rabolt, J. F. *Macromolecules* **1986**, *19*, 1725.
(18) Hicks, J. C.; Jones, T. E.; Logan, J. C. *J. Appl. Phys.* **1978**, *49*, 6092.
(19) Koizumi, N.; Hagino, J.; Murata, Y. *Ferroelectrics* **1981**, *32*, 141.
(20) Tosaka, S.; Miyata, S. *J. Appl. Phys.* **1985**, *57*, 906.
(21) Murata, Y.; Koizumi, N. *Polym. J.* **1985**, *17*, 1071.
(22) Lovinger, A. J. *Macromolecules* **1983**, *16*, 1529.
(23) Lovinger, A. J.; Johnson, G. E.; Bair, H. E.; Anderson, E. W. *J. Appl. Phys.* **1984**, *56*, 2412.
(24) Lovinger, A. J.; Davis, D. D.; Cais, R. E.; Kometani, J. M. *Macromolecules* **1986**, *19*, 1491.
(25) Lovinger, A. J.; Davis, D. D.; Cais, R. E.; Kometani, J. M. *Macromolecules* **1988**, *21*, 78.
(26) Murata, Y. *Polym. J.* **1987**, *19*, 337.
(27) Green, J.; Rabolt, J. F. *Macromolecules* **1987**, *20*, 456.
(28) Lovinger, A. J.; Davis, D. D.; Cais, R. E.; Kometani, J. M. *Polymer* **1987**, *28*, 617.
(29) Stein, R. S.; Rhodes, M. B. *J. Appl. Phys.*, *31*, 326 (1960).
(30) The OMA3 (optical multichannel analyzer, E.G.&G. PARC Model 1460-V) is a modified version of the OMA2 described in ref 28. It is equipped with a Motorola 68000 microprocessor (1.25 Mbytes RAM). It allows for collection and storage of either 50 × 50 data points (2D scan) at a rate of 2 scans/s or 500 data points (linear scan) at a rate of 1 scan every 10 ms.
(31) Tabar, R. J.; Stein, R. S.; Long, M. B. *J. Polym. Sci. Polym. Phys. Ed.* **1982**, *20*, 2041.
(32) Marand, H. L.; Klinkhammer, F.; Stein, R. S. to be submitted for publication.
(33) Tabar, R. J.; Leite-James, P.; Stein, R. S. *J. Polym. Sci., Polym. Phys. Ed.* **1985**, *23*, 2085.
(34) Prud'homme, R. E.; Stein, R. S. *J. Polym. Sci., Polym. Phys. Ed.* **1974**, *12*, 1805.
(35) Clough, S.; Rhodes, M. B.; Stein, R. S. *J. Polym. Sci., Part C* **1967**, *18*, 1.